A&A 566, A143 (2014)
DOI: 10.1051/0004-6361/201323085

Astronomy & Astrophysics

A time-dependent photochemical model for Titan's atmosphere and the origin of H_2O⋆

L. M. Lara[1], E. Lellouch[2], M. González[1], R. Moreno[2], and M. Rengel[3]

[1] Instituto de Astrofísica de Andalucía - CSIC, c/ Glorieta de la Astronomía s/n, 18008 Granada, Spain
e-mail: lara@iaa.csic.es
[2] LESIA, Observatoire de Paris-Meudon, 92195 Meudon Principal Cedex, France
[3] Max-Planck-Institut für Sonnensystemforschung, Max-Planck-Str. 2, 37191 Katlenburg-Lindau, Germany

Received 19 November 2013 / Accepted 17 April 2014

ABSTRACT

Context. Titan's stratosphere contains oxygen compounds (CO, CO_2, and H_2O), implying an external source of oxygen whose nature is still uncertain. Recent observations from the *Herschel* Space Observatory using the HIFI and PACS instruments and the *Cassini*/CIRS, as well as steady-state photochemical modeling indicate that the amounts of CO_2 and H_2O in Titan's stratosphere may imply inconsistent values of the OH/H_2O input flux, and that the oxygen source is time-variable.
Aims. We attempt to reconcile the H_2O and CO_2 observed profiles in Titan's atmosphere by using an updated photochemical scheme and developing several time-dependent scenarios for the influx/evolution of oxygen species.
Methods. We use a time-dependent photochemical model of Titan's atmosphere to calculate effective lifetimes and the response of Titan's oxygen compounds to changes in the oxygen input flux. Two variants for the C-H-O chemical network are considered. We investigate a time-variable Enceladus source and the evolution of material delivered by a cometary impact.
Results. We find that the effective lifetime of H_2O in Titan's atmosphere is only a factor of six shorter than that of CO_2 and exceeds 10 yr below 200 km. A time-variable Enceladus source, involving a decrease by a factor of 5–20 in the OH/H_2O flux over the last few centuries, shows promise in explaining the relative CO_2/H_2O profiles. However, if the previous measurements from the *Herschel* Space Observatory are representative of Titan's atmospheric water, an additional H_2O loss to the haze term is needed to bring the model in full agreement with the data. In an alternate situation, CO_2 production following a cometary impact that occurred at least 220–300 yr ago can in principle explain the CO_2 "excess" in Titan's stratosphere, but this scenario is highly unlikely, given the estimates of the impact rate at Titan.

Key words. planets and satellites: atmospheres – planets and satellites: individual: Titan – planets and satellites: composition

1. Introduction

The presence of water vapor in the stratosphere of the outer planets, as established by ISO, has raised the question of the origin of external oxygen in these reducing environments. While the gross similarity of the H_2O fluxes into the four giant planets (Feuchtgruber et al. 1997) might have been taken as evidence that micrometeorite ablation is the dominant source, recent observations, especially using the *Herschel* Space Observatory (*Herschel* hereafter), have revealed a different picture. These datasets outline the role of recent cometary impacts in delivering H_2O, CO and CO_2 to Jupiter and CO in Neptune and possibly Saturn and that of Enceladus' activity in feeding Saturn's upper atmosphere with water vapor (see Cavalié et al. 2013, and references therein).

Following the original detection by ISO (Coustenis et al. 1998), the presence of water vapor has been recently revived by measurements of the H_2O vertical profile by both *Cassini*/CIRS (Cottini et al. 2012) and *Herschel*/PACS and *Herschel*/HIFI (Moreno et al. 2012) at Titan. These studies differed significantly in the amounts of H_2O implied by typically a factor of 4–5 at 115 km. Based on photochemical modeling, Moreno et al. (2012) found that the modeled CO_2 abundance at 100–200 km is too small by a factor of ∼10 compared to the observed value of 10–20 ppb when the H_2O influx is adjusted to match their water profile. Noting that the atmospheric lifetimes of CO_2 and H_2O are very different, Moreno et al. (2012) proposed that the discrepancy could be solved by invoking a variable input flux over timescales of tens to hundreds of years and tentatively favored Enceladus' plume activity as the source of Titan's external oxygen.

Most recently, Dobrijevic et al. (2014) presented a fully coupled oxygen-nitrogen-hydrocarbon model, in which a number of reactions had been updated or added since the previous models by Hörst et al. (2008) and Moreno et al. (2012); in particular, reactions between N- and O-bearing species were considered. They confirmed the essential conclusion of Moreno et al. (2012) in that the measured H_2O profile is inconsistent with the CO_2 abundance, although the disagreement was reduced to a factor of 4. Dobrijevic et al. (2014) found that reconciliation was possible if water abundances reported by Cottini et al. (2012) are correct instead; although in this situation and for an Enceladus source, their model tended to overpredict the thermospheric abundance of H_2O when compared to the globally averaged upper limit determined by Cui et al. (2009). Dobrijevic et al. (2014) also find that the deposition altitude of the OH/H_2O flux (750 km, which is representative of micrometeorite ablation, vs. the top of the atmosphere, which is characteristic

⋆ Tables 1–3 are available in electronic form at http://www.aanda.org

of an Enceladus source) influences the flux required to reproduce the observed H_2O and CO_2 profiles and the abundance of secondary N-O and H-N-O species.

In this work, by means of a time-dependent photochemical model, we explore in more details the scenario of a variable oxygen source at Titan to see whether it is a plausible explanation to the "H_2O/CO_2 puzzle". We consider both the H_2O profiles derived from *Cassini*/CIRS (Cottini et al. 2012) and from *Herschel* (Moreno et al. 2012). In addition, we study a scenario when Titan might have suffered a cometary impact in the past by bringing oxygen species into its atmosphere.

2. Model description

The number density n at altitude z for every constituent i at time t is solved by means of the usual continuity equations in spherical geometry:

$$\frac{\partial n_i}{\partial t} = P_i - n_i l_i - \frac{1}{r^2}\frac{\partial}{\partial r}\left(r^2 \Phi_i\right), \quad (1)$$

where Φ_i can be expressed as

$$\Phi_i = -n_i D_i \left(\frac{1}{n_i}\frac{\partial n_i}{\partial z} + \frac{1+\alpha_i}{T}\frac{\partial T}{\partial z} + \frac{1}{H_i}\right) - n_i K \left(\frac{1}{n_i}\frac{\partial n_i}{\partial z} + \frac{1}{T}\frac{\partial T}{\partial z} + \frac{1}{H}\right). \quad (2)$$

The variable n_i, P_i, and l_i are the number density, volumic production rate, and volumic specific loss rate, and $r = R_0 + z$, where $R_0 = 2575$ km and z runs from 34 to 1432 km with an altitude bin size of 1 km. The parameter D_i is the molecular diffusion coefficient, T is temperature, H_i and H are the individual and atmospheric scale heights, $K(z)$ is the eddy diffusion coefficient, and, α_i is the thermal diffusion coefficient. The equations are solved for methane CH_4, methyl radical CH_3, acetylene C_2H_2, ethylene C_2H_4, ethane C_2H_6, methyl acetylene CH_3C_2H, propane C_3H_8, diacetylene C_4H_2, atomic hydrogen H, molecular hydrogen H_2, carbon monoxide CO, carbon dioxide CO_2, $O(^3P)$, formyl HCO, formaldehyde H_2CO, hydroxyl OH, CH, C_2, C_4H, C_3H_5, C_2H, $^1CH_2$, $^3CH_2$, C_2H_3, C_2H_5, $C_4H_2^*$, C_4H_3, $O(^1S)$, $O(^1D)$, CH_3O, and CH_3CO.

We use a fully implicit finite difference scheme (unconditionally stable) with a variable Δt time step to accomodate the large range of characteristic times (i.e., turbulent transport, molecular diffusion, and chemical times for all the species).

The model, which originally derives from Lara et al. (1996), has been updated in several ways. First we include new reaction rates for the hydrocarbons (see Table 1). Second, for the chemical network involving oxygen species, we consider two schemes: (i) the one from (Hörst et al. 2008, hereafter H08), which was also used by (Moreno et al. 2012, see Table 2); and (ii) a modified C-H-O chemical scheme, which results from common reactions in Dobrijevic et al. (2014) and in Hörst et al. (2008) that are updated with rate coefficients in Dobrijevic et al. (2014), and additional reactions from Dobrijevic et al. (2014) that only involve the hydrocarbons and oxygen species listed above. Specifically, this means that we ignore reactions coupling N and O chemistry. This is justified by the fact that we are primarily interested by the profiles of CO_2 and H_2O and not the abundances of secondary N-O-H species. In particular, the reaction OH + $N(^4S)$ in the reaction scheme coupling N and O species (which in the C-H-N-O chemistry by Dobrijevic et al. (2014) is important above 1000 km to produce NO) only represents 0.003% of the OH column integrated loss in the C-H-O chemical network for typical OH and $N(^4S)$ vertical profiles. Regarding water, the main additional loss term that involves nitrogen is $H_2O + N(^2D)$, but this only accounts for 0.85% of the total water loss rate given typical profiles of H_2O and $N(^2D)$. Reactions for this simplified chemical scheme (hereafter L14), with regard to Dobrijevic et al. (2014) are listed in Table 3.

Finally, compared to Lara et al. (1996), a more recent treatment of the UV transmission in the haze layer is considered. For this, we have adopted the results shown in Fig. 2 of Krasnopolsky (2009), which in fact do not noticeably differ from the approximation seen in Yung et al. (1984) as used in Lara et al. (1996) and in Moreno et al. (2012).

Here we retain the same treatment for the condensation processes, as in Lara et al. (1996), and adopt the eddy diffusion coefficient (K_2) from Moreno et al. (2012), Following Hörst et al. (2008), the $O(^3P)$ flux is introduced in the model in a layer with a peak at 1100 km. The magnitude of the $O(^3P)$ flux normally drives the CO abundance. However, due to its extremely long lifetime (several 10^8 yr), reaching a chemical balance on CO needs a long integration time (e.g. Dobrijevic et al. 2014). Instead the CO mixing ratio is prescribed hereat its observed value, 5.1×10^{-5} (Gurwell 2004), at the model's lower boundary; the abundance vertical profile is then computed in the model, and the $O(^3P)$ flux is then unimportant for determining the CO_2 and H_2O profiles. As detailed below, we investigate the sensitivity of the results to form (OH vs. H_2O) and the deposition profile of the water influx.

Boundary conditions at 34 km are set as follows: for condensible species, the mixing ratio is the maximum value allowed by the saturation laws, which is zero supersaturation; for non-condensible species, either they are in local photochemical equilibrium and the number density is computed as the quotient of the production and specific loss, or they have a maximum flux through the lower boundary. At 1432 km, only H and H_2 are allowed to escape according to the Jeans formulation, whereas the other species are in diffusive equilibrium (excluding OH/H_2O in the case that they have an inward flux due to the Enceladus plume activity).

The thermal profile used for our computation is a combination of (i) the temperatures measured by Huygens/HASI (Fulchignoni et al. 2005) in the troposphere at altitudes between 0–140 km; (ii) the disk-averaged *Cassini*/CIRS stratospheric temperatures (Vinatier et al. 2010) at altitudes between 140–500 km; (iii) the *Cassini*/INMS retrieved temperatures (i.e. 155 K as average, de La Haye et al. (2007)) at altitudes between 1000–1500 km; and (iv) a decreasing temperature from 165 K to 155 K at altitudes between 500 and 1000 km.

Our study aims at reproducing (i) the H_2O vertical profiles in Moreno et al. (2012) and Cottini et al. (2012) with both chemical schemes, for H08 and L14; and (ii) the CO_2 stratospheric abundance from *Cassini*/CIRS data (de Kok et al. 2007).

3. OH versus H_2O external source

Both Hörst et al. (2008) and (Moreno et al. 2012, who considered the H08 chemical scheme) concluded that the OH vs. H_2O form of the water input is unimportant when fitting the stratospheric water abundance, since a balance is established between OH and H_2O, due to the photolysis of water and reactions between OH and CH_3 or OH and CH_4 recycling water. They also found that fluxes required to reproduce a given H_2O profile are independent on the precise deposition profile (i.e., deposition at the top of the atmosphere as appropriate or in a Chapman

Table 4. Steady-state models results for an OH and H_2 flux at the top of the atmosphere.

Observed profile	Chemical network	OH flux (cm^{-2} s^{-1})	H_2O (cm^{-2} s^{-1})	$O(^3P)$ flux (cm^{-2} s^{-1})	CO_2 mixing ratio at 150 km
S_a (Moreno et al. 2012)	H08	2.4×10^5	0	1.6×10^6	6.2×10^{-10}
S_a (Moreno et al. 2012)	L14	3.2×10^5	0	1.6×10^6	8.7×10^{-10}
S_a (Moreno et al. 2012)	L14	0	2.6×10^5	1.6×10^6	8.7×10^{-10}
CIRS (Cottini et al. 2012)	H08	9.0×10^5	0	1.0×10^6	2.5×10^{-9}
CIRS (Cottini et al. 2012)	L14	1.2×10^6	0	1.6×10^6	3.3×10^{-9}
CIRS (Cottini et al. 2012)	L14	0	9.8×10^5	1.6×10^6	3.3×10^{-9}

layer near 750 km). On the other hand, Dobrijevic et al. (2014) found large variations in the required H_2O/OH flux depending on its H_2O vs. OH form and on its altitude deposition. For example, Table 2 of Dobrijevic et al. (2014) shows that a given flux produces ~33% more H_2O in Titan's atmosphere for meteoritic ablation near 750 km (cases "IM1" and "IM4"), when it is deposited in the form of H_2O compared to the case where it is deposited as OH. The difference becomes larger in the case of water deposition at the top of the atmosphere (cases "IE1" and "IE2"), where a OH flux (compared to H_2O flux) that is twice as large is needed to produce the same amount of H_2O.

We re-examined these issues with the new treatment of the UV transmission within the haze and the new chemical network (L14). For this, we computed steady-state solutions by fine-tuning the OH/H_2O influx to match the available observations (HIFI+PACS in Moreno et al. (2012) and *Cassini*/CIRS by Cottini et al. (2012)). Table 4 summarizes the required fluxes to match the H_2O determinations from *Herschel* and *Cassini*/CIRS by using the two sets of chemistry and water influx in the form of either OH or H_2O. (Only cases of deposition at the top of the atmosphere are summarized in Table 4.)

Although we do find with our simplified L14 scheme values that are similar to Dobrijevic et al. (2014), Table 4 indicates that an influx in the form of H_2O entering Titan's atmosphere is more "efficient" at producing H_2O in Titan's atmosphere than an OH flux; the difference is only about 20% (vs. a factor ~2 in Dobrijevic et al. 2014). Moreover, for a given form of deposition (OH or H_2O), we do not find any significant difference between the required fluxes as a function of deposition profile, as the associated Titan H_2O profiles for a given flux and the two scenarios of deposition profiles are identical up to 750 km. In contrast, the profiles start to diverge above this altitude as seen in Figs. 12 and 13 of Moreno et al. (2012), so that measurements of the H_2O mole fraction in the upper atmosphere could help constrain the Enceladus in contrast to micrometeoroid ablation origin of the external flux. We are unsure of the cause of the discrepancy with Dobrijevic et al. (2014), and we do not understand why their required fluxes are so dependent on the altitude deposition profile. Indeed, we estimated that the non-inclusion of the N-O coupling has a negligible effect of the fluxes required to match a given H_2O profile above, and the latter authors do not explicitly show a case with the N-O chemistry turned off for comparison. Likely reasons of the discrepancy may be related to significantly different profiles of the C-H and C-H-N species profiles computed in (Dobrijevic et al. 2014, not shown therein) and ours.

4. Lifetimes

Moreno et al. (2012) could not simultaneously fit the stratospheric abundance of H_2O measured with *Herschel* and of CO_2 (de Kok et al. 2007) with the same OH and $O(^3P)$ flux. They proposed that the discrepancy could be solved by invoking a time-variable input flux. They based their argument on the different atmospheric lifetimes of H_2O and CO_2. This had been already found by Wilson & Atreya (2004), who reported chemical lifetimes of 4.1 and 697 yr at 300 km for H_2O and CO_2. Moreno et al. (2012) obtained similar numbers (9 yr and 450 yr) for the "column-integrated" lifetime, which is defined by dividing the column density by the vertically-integrated chemical loss including photolysis. For CO_2, this lifetime was comparable to the vertical transport time down to the condensation level (360 yr). However, these approaches give either an estimate of the lifetime against chemical loss at some level or a global estimate of the atmospheric residence time of a species in the atmosphere, but they do not handle the fact that the time evolution of the atmospheric mixing ratios depends on both chemical and transport processes, which may show important variations with altitude.

To account for this, we first used our time-dependent model as described, to study the response of oxygen species to an abrupt change in the oxygen source rate. For this, we initialized the oxygen compounds to the steady state solution profiles obtained in the case of the OH Enceladus source (i.e, deposited at the top of the atmosphere) by considering the two variants of the oxygen chemistry (H08 and L14). The steady state OH fluxes required to match the H_2O *Herschel* profile are given in Table 4, and an $O(^3P)$ flux of 1.6×10^6 cm^{-2} s^{-1} is used. Then, for each case, the oxygen sources are cut to zero and the oxygen species evolve with time. For each species, we define the altitude-dependent "effective lifetime" as the time after which the mixing ratio has decreased by a factor e at the considered altitude. This definition is clearly only approximate since the time evolution does not follow a simple exponential decay. Results for the H08 chemical network are shown in Fig. 1 for all oxygen species but CO (which has a very long lifetime at all levels). It has to be pointed out that the "effective lifetimes" for every species are approximately the same when using the H08 or the L14 chemical network.

For comparison, Fig. 2 shows the altitude-dependent lifetimes associated to the different processes considered in the model for some oxygen species (CO_2, H_2O, H_2CO, $O(^3P)$ and OH): photolysis, gas-gas chemical reactions (for which the lifetime is defined at each altitude j as the minimum of $1/l^k_{i,j}$, k that represents all of the reactions consuming the species i at altitude j), molecular diffusion, and turbulent transport. For H_2O, the photolytic lifetime (which drives the overall chemical lifetime) increases from ~0.5 yr at the top of the atmosphere to ~10 yr at 200 km and further increases at lower levels. The ratio of the chemical lifetime of CO_2 to that of H_2O is a factor of 100 above 400 km. All these numbers are consistent with the above estimates of the "column-integrated" chemical lifetimes.

Nonetheless, the time evolution of the at a given level is more properly described by the effective lifetimes (Fig. 1). For H_2O, it increases regularly from ~0.1 yr at the top to 10 yr

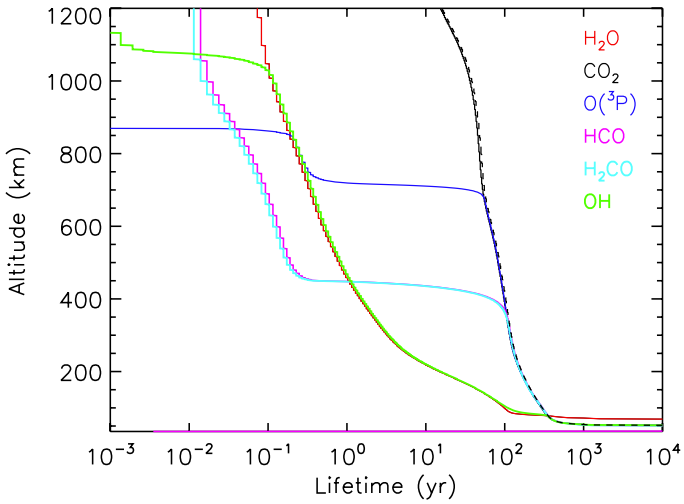

Fig. 1. Effective lifetimes (see text for definition) as a function of altitude for oxygen species. These are calculated for OH and O(^{3}P) input fluxes of 2.4×10^5 and 1.6×10^6 cm^{-2} s^{-1}, respectively, and the H08 chemical network. The effective lifetime for CO_2 for an enhanced input OH flux = 5.1×10^6 cm^{-2} s^{-1} (needed to match the CO_2 profile) is also shown as a dashed black line.

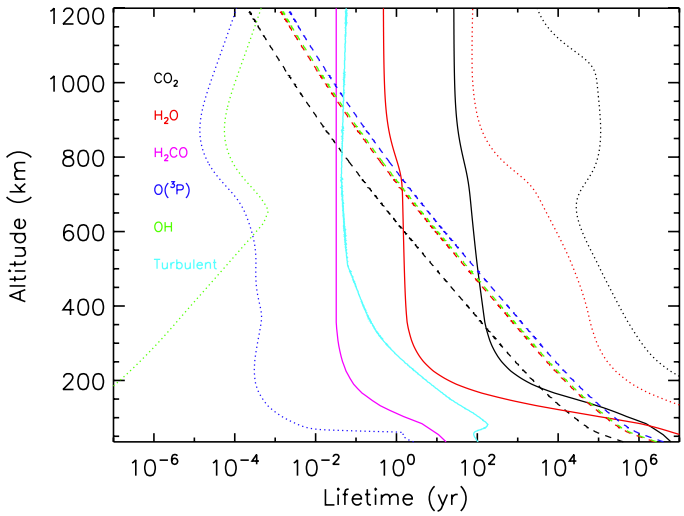

Fig. 2. Lifetimes for different processes. Solid lines: photolytic lifetime Dotted lines: chemical (gas-gas) lifetime. Dashed lines: molecular diffusion timescale. (H_i^2/D_i). The characteristic time for turbulent transport (H^2/K) is also shown. This figure makes use of the H08 chemical scheme, where OH photolysis is not included, and H_2CO is only lost via photodissociation.

at 200 km and about 100 yr at 80 km (at deeper levels, H_2O is constrained to very small amounts by condensation, so the apparent "divergence" of the lifetime is not meaningful). For CO_2, the effective lifetime increases from 20 yr at the top of the atmosphere to 400 yr at ~80 km before entering in the condensation region. The OH lifetime is very short in the upper atmosphere (>1000 km) but it tracks that of H_2O from which it is photochemically produced below this altitude. Similarly, the lifetimes of O(^{3}P) and HCO/H_2CO are short below 850 and 450 km and progressively increase to follow that of CO_2 below 700 and 400 km, respectively. For these four species, the long lifetimes in the lower atmosphere have, however, little significance because the involved amounts are very small. In addition to the altitude-dependent effective lifetime, it is useful to similarly define the column-averaged effective lifetime as the time after which the column density has decreased by a factor e. These column-average lifetimes are found to be 287 yr, 51 yr, 12 d, 10 d, 5 h, and 1 h for CO_2, H_2O, H_2CO, HCO, OH, and O(^{3}P), respectively. The most important result for our purpose is that the effective lifetimes for CO_2 and H_2O differ by less than a factor of 6, regardless of the photochemical scheme and the initial profile to which time-evolution is applied.

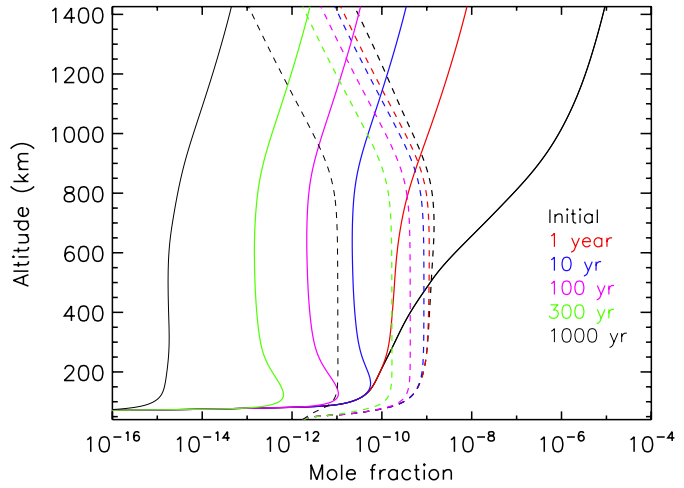

Fig. 3. Time-evolution of oxygen species 1, 10, 100, 300 and 1000 yr after the oxygen sources have been abruptly cut-off. Profiles are initialized at steady-state conditions for O(^{3}P) and OH input fluxes at 1.6×10^6 and 2.4×10^5 cm^{-2} s^{-1}, respectively, matching the H_2O profile of Moreno et al. (2012). Solid lines refer to H_2O, and dashed lines refer to CO_2.

5. Evolution of the H_2O and CO_2 profiles under changes of the input flux

Running the time-dependent model shows that all species except CO, CO_2, and H_2O decrease to molar fractions $<10^{-12}$ in less than 10 yr upon an abrupt cut-off of the oxygen input fluxes. While the shape of the CO_2 profile is conserved as the CO_2 abundance slowly declines with time, the H_2O profile strongly evolves. As a consequence of the quick altitude-varying lifetime, the H_2O depletion proceeds much more rapidly at upper levels, causing a local maximum ("kink") of the H_2O mixing ratio in the 125−160 km altitude range to appear after ~10 yr. This behavior occurs for both the H08 and L14 chemical networks, and initial water profiles in agreement with either *Herschel* or *Cassini*/CIRS data. Figure 3 shows the evolution of the CO_2 and H_2O profiles for initial conditions that match the S_a profile in Moreno et al. (2012) and adopt the H08 chemistry.

5.1. Time-variable input fluxes

Builiding on this, we considered a simple scenario for the time evolution of the oxygen fluxes to test the hypothesis of a time-variable Enceladus source being responsible for the "inconsistent" H_2O and CO_2 abundances. Essentially, we assume that the input fluxes have been strong enough in the past to explain the observed CO_2 and that they have decreased exponentially since some recent time. We describe the history of the OH flux as

- for $t <$ current epoch–t_0: $\Phi(\mathrm{OH}) = \Phi_0(\mathrm{OH})$;
- for $t >$ current epoch–t_0: $\Phi(\mathrm{OH}) = \Phi_0(\mathrm{OH}) \times \exp(-(t/\tau))$,

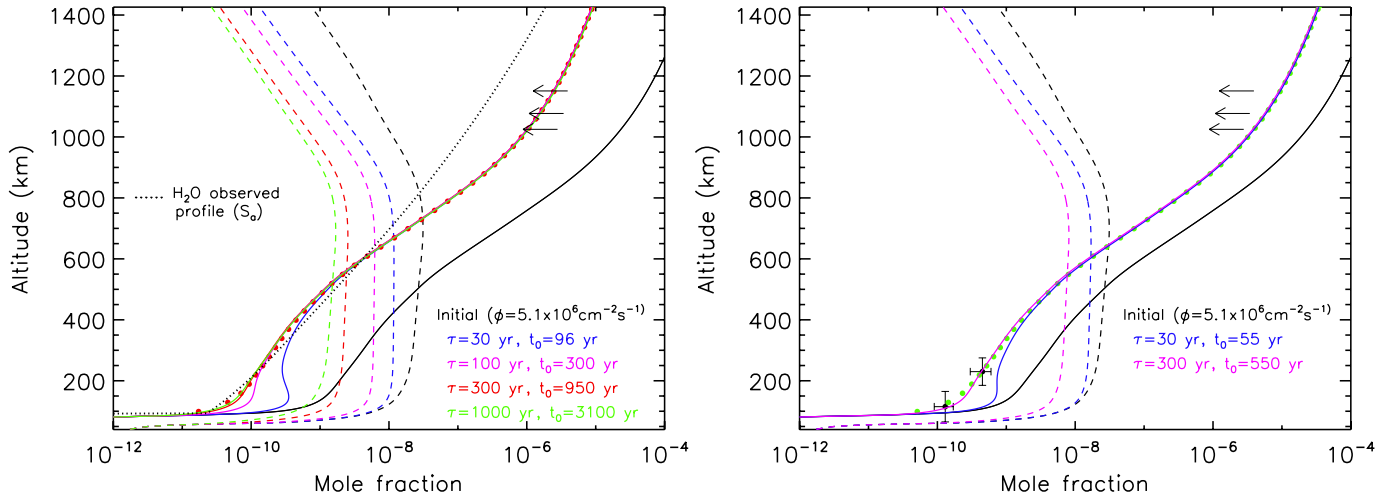

Fig. 4. H_2O (solid lines) and CO_2 (dashed lines) profiles in a time-dependent Enceladus source model, as compared to observations, making use of the H08 chemical scheme. *Left panel*: results aimed at fitting the H_2O observed with *Herschel*. The profiles are initialized at their steady-state values for a OH flux of 5.1×10^6 cm^{-2} s^{-1} (black curves). The different curves correspond to evolution with four different combinations of τ and t_0. The red circles show the H_2O profile in the (τ = 30 yr, t_0 = 96 yr) case calculated in presence of an additional loss of H_2O to the haze (see text). *Right panel*: results aimed at fitting the H_2O observed with *Cassini*/CIRS. The black curves correspond to the steady state profiles obtained with an OH flux of 5.1×10^6 cm^{-2} s^{-1}. Evolution of these profiles for two different (τ, t_0) combinations are shown, as well as the resulting H_2O profile, when a loss to the haze is taken into account for the (τ = 30 yr, t_0 = 55 yr) case (green dots). Upper limits on H_2O thermospheric abundance by Cui et al. (2009) are also shown as arrows.

where t is the time elapsed since the onset of the flux decline, which is assumed to have started t_0 yr before the current epoch. The model thus has three free parameters: (i) t_0, the number of years in the past when the input fluxes have started to decrease; (ii) Φ_0(OH), the input flux before it started to decrease; and (iii) τ, the characteristic time of the flux decline. Since we are modeling an Enceladus source, we assume that the O(^{3}P) flux follows the same time dependence and fix the O(^{3}P)/OH flux ratio to a constant value.

In the first step, we fixed Φ_0(OH) at the value required to match the observed CO_2 mole fraction of 1.5×10^{-8} at 100–200 km in a steady-state situation. This Φ_0(OH) flux depends slightly on the photochemical network, being 5.1×10^6 cm^{-2} s^{-1} for H08 and 5.3×10^6 cm^{-2} s^{-1} for L14. These values are 16–20 times larger than the steady-state flux needed to match the H_2O profile of Moreno et al. (2012) and 4–5.5 times larger than that required to match the H_2O profile of Cottini et al. (2012). In the middle/upper atmosphere (say above 300 km), the lifetime of H_2O is short, so that the H_2O mole fraction reacts to the "instantaneous" flux. This essentially constrains the flux to have declined by the above factors, which implies t_0/τ = 2.9–3.2 if the water targeted profile is S_a in Moreno et al. (2012) and t_0/τ = 1.5–1.8 if the H_2O abundance to be reproduced is from *Cassini*/CIRS data (Cottini et al. 2012). The value of τ (and hence t_0) remains to be adjusted. However, the CO_2 abundance, which reflects the input flux that is "smoothed" over ~300 yr, and the profile of H_2O below 300–400 km, tend to provide contradictory constraints. Short values of τ and t_0 are favored by CO_2, while the steep H_2O slope (i.e., the absence of a "kink" near 150 km) would rather point to long values of τ and t_0. Figure 4 shows the profiles of H_2O and CO_2 for various (τ, t_0) combinations aimed at reproducing:

- (left panel): H_2O from *Herschel* (Moreno et al. 2012) and CO_2 from *Cassini*/CIRS observations (de Kok et al. 2007), and
- (right panel): H_2O and CO_2 from *Cassini*/CIRS observations (Cottini et al. 2012; de Kok et al. 2007).

In the first case (target H_2O profile = S_a from Moreno et al. (2012)), the (τ = 30 yr, t_0 = 96 yr) combination permits to reproduce a CO_2 profile that closely agrees with its observed value, but the H_2O profile shows a marked local maximum and an abundance that is too large below 250 km. Conversely, for (τ = 1000 yr, t_0 = 3100 yr), the H_2O profile is adequate, but CO_2 is underabundant by a factor of 10. Intermediate sets of parameters, such as (τ = 100 yr, t_0 = 300 yr) or (τ = 300 yr, t_0 = 950 yr), produce unsatisfactory compromises with a poor fit for both species.

The same general conclusion can be seen in the right panel of Fig. 4, where the target H_2O profile is now taken from Cottini et al. (2012). For (τ = 30 yr, t_0 = 55 yr), the CO_2 stratospheric value is close to the measurements, but the water profile sharply overestimates the H_2O mixing ratio near 125 km. For (τ = 300 yr, t_0 = 550 yr), H_2O is brought into agreement with *Cassini*/CIRS results, but CO_2 is considerably below observations.

As can be seen on the right panel of Fig. 4, the models tuned to match the H_2O abundance somewhat overestimate the upper limits (2.8×10^{-6} up to 3.9×10^{-6} in the 1025–1151 km region) from INMS (Cui et al. 2009). A similar problem was encountered by Dobrijevic et al. (2014) for an Enceladus source. We note, however, that Cui et al. (2009) report actual detections of H_2O on several inbound spectr with H_2O mixing ratios in the range $(0.4–3.4) \times 10^{-5}$ with a mean value of 1.2×10^{-5}. These mixing ratios would then be consistent with model predictions, so the resolution of this issue must await a clarification of the constraints from INMS. At any rate, we note that the H_2O thermospheric abundance is sensitive to the precise OH vs. H_2O and vertical deposition profile and might also be affected by reactions (not considered here) that couple the O and N chemistry. In contrast, these effects do not affect the H_2O and CO_2 stratospheric abundances.

The above models assumed an initial Φ_0(OH) equal to the steady-state value needed to fit the CO_2 abundance. We explored alternative models with a higher value for Φ_0(OH). Specifically

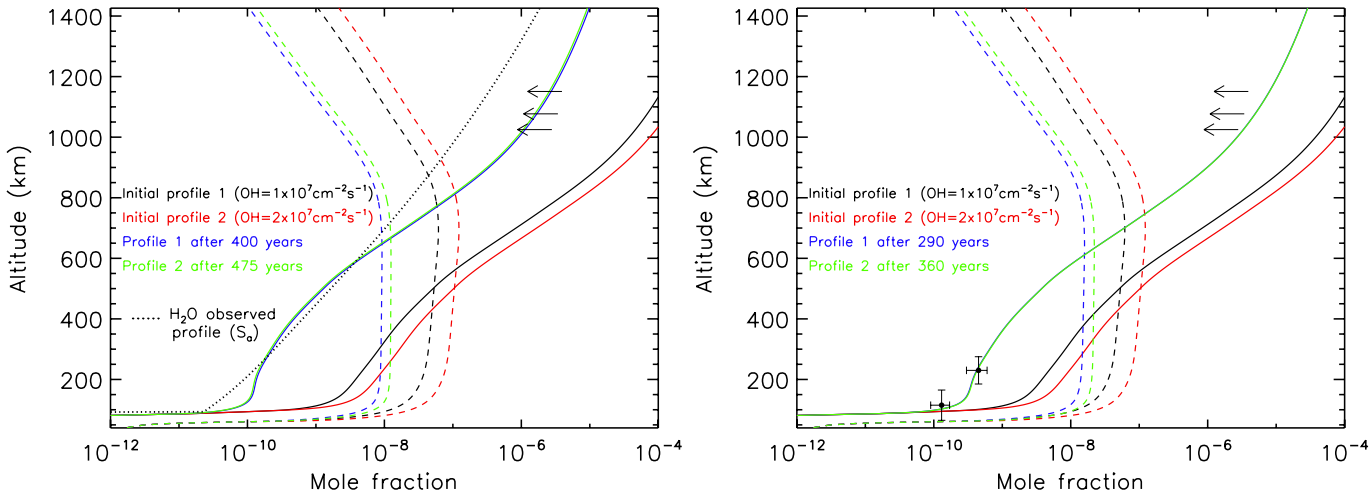

Fig. 5. H_2O (solid lines) and CO_2 (dashed lines) profiles in a time-dependent Enceladus source model (H08 chemistry) compared to the observed profile of H_2O from (i) *left panel*: *Herschel* (S_a profile from Moreno et al. (2012); and (ii) *right panel*: *Cassini*/CIRS (Cottini et al. 2012) . Two initial conditions with different and enhanced OH input fluxes (1.0×10^7 in black lines and 2.0×10^7 cm^{-2} s^{-1} in red lines) are considered. Evolution times are adjusted so that the H_2O mole fraction above 300 km matches observations in the case of *Herschel* data and at 230 km in the case of *Cassini*/CIRS. The resulting (i.e., after t_0 yr of evolution) H_2O and CO_2 profiles are plotted with blue and green lines for the initial profiles 1 and 2, respectively (see text for more details). Upper limits on H_2O thermospheric abundance by Cui et al. (2009) are also shown as arrows.

Table 5. Evolution time t_0 required to match the *Herschel* or *Cassini*/CIRS H_2O profiles for both chemical schemes (H08 or L14).

Φ_0(OH) (cm^{-2} s^{-1})	H08 chemical scheme		L14 chemical scheme	
	Herschel[a]	*Cassini*/CIRS	*Herschel*[a]	*Cassini*/CIRS
1.0×10^7	400	290	375	260
2.0×10^7	475	360	450	330

Notes. The time constant of the flux decline is τ = 100 years. [(a)] Poor fit.

with the H08 chemical scheme, we considered two cases with initial fluxes of Φ_0(OH) = 1.0×10^7 and 2.0×10^7 cm^{-2} s^{-1}, respectively, that then declined with a time constant τ = 100 yr. The evolution time t_0 needed to match the H_2O *Herschel* abundance above 300 km altitude is 400 yr and 475 yr for the two cases, respectively. As shown in Fig. 5 (left panel), this scenario maintains larger CO_2 values compared to the τ = 100 yr case shown in Fig. 4 (which had t_0 = 300 yr and Φ_0(OH) = 5.1×10^6 cm^{-2} s^{-1}). The Φ_0(OH) = 2.0×10^7 cm^{-2} s^{-1} case yields CO_2 abundances that are essentially consistent with the observed $\sim1.5\times10^{-8}$ value at 100–200 km. However, the corresponding H_2O profile still shows some "kink" below 200 km. Direct comparison of synthetic spectra with data from Moreno et al. (2012) indicates that it still overpredicts the PACS lines (which probe the 90–150 km range) by ~50% while the H_2O model correctly fits the HIFI observations.

On the other hand, the same approach provides a satisfactory match to the *Cassini*/CIRS H_2O measurements at 115 and 230 km. Continuing with the same chemical scheme, initial Φ_0(OH) fluxes, and τ = 100 yr, we find that the Cottini et al. (2012) H_2O profile can be reproduced with t_0 = 290 yr for Φ_0(OH) = 1.0×10^7 cm^{-2}s^{-1} and t_0 = 360 yr for Φ_0(OH) = 2.0×10^7 cm^{-2} s^{-1} (see Fig. 5, right panel). In both cases, the resulting CO_2 stratospheric profile agrees well with observations.

We performed the same exercise by using the alternate chemical network (L14). Keeping the characteristic time of the flux decline at τ = 100 years, Table 5 summarizes the required values of the evolution time t_0 for the different cases. Similar behaviors are obtained with the two sets of chemistry. We conclude that this family of solutions is not satisfactory if the targeted water profile is the one retrieved from *Herschel* data, whereas a more successful fit of *Cassini*/CIRS water and carbon dioxide is obtained by assuming considerably OH higher fluxes some centuries ago.

5.2. Loss to the haze

Moreno et al. (2012) speculated that the H_2O profile could be affected by an additional non-gaseous chemical loss, which can be a loss to the haze, as it seems to the case for HCN (McKay 1996; Lara et al. 1999; Vinatier et al. 2007). Moreno et al. (2012) found that adding a loss term in the form of $L = k[H_2O]^{1.75}$ cm^{-3} s^{-1} restricted to altitudes above 220 km would bring the model to the calculated H_2O profile in agreement with the *Herschel* observations. However, they discarded this option because it does not help reconcile in itself the H_2O and CO_2 profiles in the steady-state scenario considered in Moreno et al. (2012).

Nonetheless, in this time-dependent scenario, a loss to the haze potentially reduces the H_2O mole fraction in the lower stratosphere, as eliminates the H_2O "kink" near 150 km and recoves an H_2O profile in light with the *Herschel* observations. To illustrate this, here we come back to the short evolution case of Fig. 4 (left panel) (having Φ_0(OH) = 5.1×10^6 cm^{-2} s^{-1}, τ = 30 yr, t_0 = 96 yr), add a loss term of H_2O to the haze in the form $L = k[H_2O]^\beta$ cm^{-3} s^{-1} at $z > 300$ km, which decreases with a −100 km scale height below 300 km. In a nominal case, we adopt β = 1.75 by analogy to results of HCN (Lara et al. 1999),

Table 6. Models with H_2O loss to the haze.

Φ_0(OH) (cm^{-2} s^{-1})	Chemical network	Target H_2O profile	(t_0, τ) (year)	(k, β)	CO_2 mixing ratio at 150 km	H_2O integrated loss to the haze (cm^{-2} s^{-1})
5.1×10^6	H08	*Herschel*	(96, 30)	$(5.0 \times 10^{-16}, 2)$	9.3×10^{-9}	5.9×10^5
				$(2.0 \times 10^{-14}, 1.75)$	9.2×10^{-9}	6.5×10^5
		Cassini/CIRS	(55, 30)	$(1.5 \times 10^{-16}, 2)$	1.2×10^{-8}	2.2×10^5
				$(1.0 \times 10^{-14}, 1.75)$	1.2×10^{-8}	2.5×10^5
5.3×10^6	L14	*Herschel*	(87, 30)	$(5.0 \times 10^{-16}, 2)$	9.9×10^{-9}	6.1×10^5
				$(2.0 \times 10^{-14}, 1.75)$	9.8×10^{-9}	6.8×10^5
		Cassini/CIRS	(45, 30)	$(1.5 \times 10^{-16}, 2)$	1.2×10^{-8}	2.5×10^5
				$(1.0 \times 10^{-14}, 1.75)$	1.2×10^{-8}	2.8×10^5

but solutions with different forms are possible. The red circles in the left panel of Fig. 4 show the resulting H_2O profile obtained with $k = 2 \times 10^{-14}$. This profile fully agrees with the empirical S_a profile of Moreno et al. (2012). Alternate functional dependences of L are possible; for example, $L = k'[H_2O]^2$ cm^{-3} s^{-1} with $k' = 5 \times 10^{-16}$ at $z > 300$ km and similarly decreases below this altitude produces an identical fit. In these models, the total H_2O loss to the haze is $\sim 6 \times 10^5$ cm^{-2} s^{-1}.

For completeness, this study has been extended to the case of the H_2O *Cassini*/CIRS profile and also considers the two chemical schemes. Table 6 shows results of the (k, β) parameters and the total H_2O loss to the haze for the different cases.

As a conclusion, including a loss to the haze term in combination on with a time variable flux brings the modeled H_2O profile in agreement with available observations (Cottini et al. 2012; Moreno et al. 2012) for both of the chemical schemes used here, which maintains CO_2 stratospheric profiles in broad agreement with *Cassini*/CIRS data (de Kok et al. 2007).

6. Comet impact scenario

In this section, we investigate another alternative for the high CO_2/H_2O ratio in Titan's atmosphere: namely, the CO_2 that has built up from a relatively recent cometary impact. As shown from the Shoemaker-Levy 9 impacts on Jupiter in 1994, cometary impacts can deliver oxygen compounds to planets. In the Jupiter/SL9 case, shock chemistry at plume re-entry has produced CO and H_2O near the 0.1 mbar level (Lellouch et al. 1997, 2002), and both species have since then slowly diffused vertically and horizontally (see Moreno et al. 2003; Cavalié et al. 2013, and references therein). Furthermore, while CO is chemically stable, any newly injected H_2O is progressively photolysed to OH and converted to CO_2 by reaction with CO. The gas CO_2 was observed in 1997 in Jupiter (Lellouch et al. 2002) with a north-south assymetry characteristic of a SL9-derived product (Lellouch et al. 2002). Based on coupled photochemical-horizontal transport modeling, the amount of carbon dioxide and latitudinal distribution could be explained if the material produced by the impacts has a H_2O/CO ratio of about 0.11 per volume. In Jupiter's atmosphere, the model further predicted that CO_2 produced in this manner would build up for about 50 yr after the impacts and then begin to decline due to its own photolysis. Comet impacts are also invoked to explain the abundance of CO in Neptune's stratosphere (Lellouch et al. 2005; Hesman et al. 2007) and possibly Saturn's (Cavalié et al. 2010).

We first examine the scenario for Titan in terms of the involved amounts. The CO_2 column density in Titan's atmosphere is 3.6×10^{16} cm^{-2} which corresponds to 3.0×10^{34} molecules referred to the surface. Assuming full conversion of H_2O to CO_2 and using an initial H_2O/CO ratio of 0.1, this implies that the hypothetical comet delivered 3.0×10^{34} H_2O and 3.0×10^{35} CO molecules (i.e, a CO mass of 1.4×10^{13} g). Converting this CO mass into a comet size requires an assumption of the "CO yield" and the comet density. We use a 50% yield (Lellouch et al. 1997, 2005) and a 0.5 g cm^{-3} mass density. This gives a minimum $D = 0.475$ km comet diameter.

We then consider the time evolution of a "pure" cometary case, by first considering the constraints from the H_2O *Herschel* profile. The CO and H_2O mole fractions are initialized as q_{CO} and q_{H_2O}, which are taken as uniform above 300 km (0.1 mbar) and zero below this altitude. These values are considered as constant over the Titan globe. Thus the model is not initialized at comet impact, but a few years after when the species have been mixed horizontally and vertically above the 300 km range ($q = q_{CO}$). We impose $q_{CO} = 10 \times q_{H_2O}$, and these values are adjusted until the CO_2 mole fraction matches the observations after some evolution time t_{evol}. Figure 6 (left panel) shows two cases (both of which consider the H08 chemical network): (1) $q_{CO} = 6 \times 10^{-5}$, $t_{evol} = 300$ yr; and (2) $q_{CO} = 6 \times 10^{-4}$, $t_{evol} = 700$ yr. These two cases correspond to the deposition of 1.2×10^{36} and 1.2×10^{37} CO molecules implying a cometary diameter of 0.7 and 1.5 km ("small" and "large"), respectively, under the above assumptions on density and CO yield. Both cases produce roughly the same amount of CO_2; in contrast, a significantly larger amount of H_2O is present in the first case, although this amount of water is importantly below the *Herschel* observations in both cases. Case (1) represents the maximum amount of cometary H_2O that can be accomodated by the observed *Herschel* H_2O profile. This implies that the comet impact occured at least 300 yr ago with a minimum comet diameter of 700 m. Older impacts are possible but require larger impactor sizes to maintain the same amount of CO_2.

The right panel of Fig. 6 shows similar models but are tailored to the *Cassini*/CIRS H_2O profile. The "large" comet case is unchanged, but the "small" comet case has values of $q_{CO} = 3 \times 10^{-5}$, $t_{evol} = 225$ yr. Indeed, the larger stratospheric abundance in the *Cassini*/CIRS H_2O profile can accomodate a larger residual cometary H_2O than the *Herschel* profile. This can be achieved by invoking a smaller and more recent impact (leading to the same CO_2 amount but a larger H_2O/CO_2 ratio after evolution). As it is clear in the right panel of Fig. 6, this case is close to the maximum value of cometary H_2O that can be tolerated by the observed *Cassini*/CIRS H_2O profile. This means that if the *Cassini*/CIRS H_2O profile is valid, the impact age could be as young as 225 years with the minimum size of 550 m. Again, older and larger impacts are possible.

We can also combine one of the above models with steady-state production of the oxygen species. This scenario thus

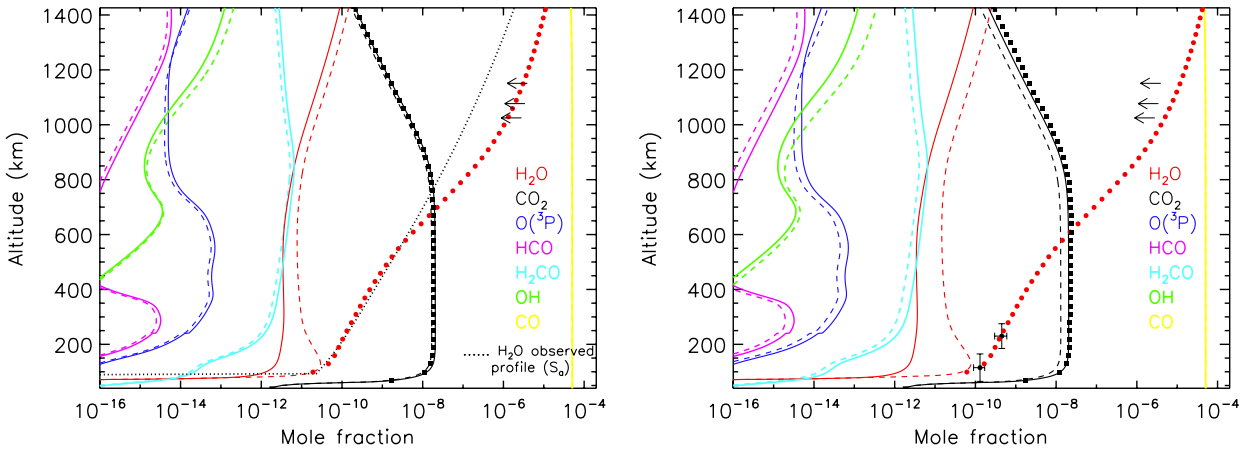

Fig. 6. Evolution of oxygen species after a cometary impact. Initial conditions correspond to deposition of CO and H_2O with uniform mixing ratios (with $q_{CO} = 10\ q_{H_2O}$) above 300 km. *Left panel*: models suited to the *Herschel* H_2O profile (S_a from Moreno et al. (2012)). Dashed lines: "small comet" (initial $q_{CO} = 6 \times 10^{-5}$), evolution time $t_{evol} = 300$ yr. Solid lines: "large comet" (initial $q_{CO} = 6 \times 10^{-4}$), evolution time $t_{evol} = 700$ yr. The red circles and black squares show the H_2O and CO_2 for the combination of the "large comet" case with a steady OH influx of 2.4×10^5 cm^{-2} s^{-1}. *Right panel*: models suited to the *Cassini*/CIRS H_2O profile Cottini et al. (2012). Dashed lines: "smaller comet" (initial $q_{CO} = 3 \times 10^{-5}$), evolution time $t_{evol} = 225$ yr. Solid lines: "large comet" (initial $q_{CO} = 6 \times 10^{-4}$), evolution time $t_{evol} = 700$ yr. The red circles and black squares show the H_2O and CO_2 for the combination of the "large comet" case with a steady OH influx of 9.0×10^5 cm^{-2} s^{-1}. Upper limits on H_2O thermospheric abundance by Cui et al. (2009) are also shown as arrows.

depicts the current abundance of oxygen species as a result from the combination of a steady (Enceladus or micrometeorite) source and the evolution of a cometary "spike". The steady source is primarily responsible for the H_2O abundance, while CO_2 is mostly the result of the comet impact. The dotted lines in Fig. 6 show the combination of the "large comet" above case with an Enceladus source (with a steady OH source rate of 2.4×10^5 cm^{-2} s^{-1} in the left panel and 9.0×10^5 cm^{-2} s^{-1} in the right panel). The resulting H_2O profiles after 700 yr evolution agree with *Herschel* and *Cassini*/CIRS observations, respectively, and the CO_2 profile is also fit.

The use of the alternate (L14) oxygen chemical scheme does not noticeably influence the results above. Matching the observations for the same model assumptions in terms of comet size and evolution time only requires a slight ($\leq$10%) increase of the Φ_{OH} that is provided by the steady Enceladus source. This is to be expected from Table 4, which shows the L14 oxygen chemical scheme to be slightly less efficient in producing atmospheric water.

While these models "technically' work, their main difficulty is in the plausibility of a recent impact at Titan. Zahnle et al. (2003) find that the number of impacts on Jupiter by 1.5 km or larger ecliptic comets is typically 0.005 per year. They further provide probabilities for ecliptic comet impacts relative to Jupiter for all outer planets and satellites. For Titan, this relative probability is given as 5.4×10^{-5}, which means that Titan is hit by a $D > 1.5$ km comet every ~4 million years on average. The size distribution of the cumulative impact rate is not very steep (slope parameter $b = 1-1.7$ in this size range, according to Zahnle et al. 2003), which means that the occurrence of a 0.5 km comet impact at Titan is only 3–6 times larger. We are still left with typical impact times of ~1 million years, which is probably fatal for this scenario.

7. Conclusions

We have explored Titan oxygen photochemistry by using a time-variable photochemical model and considering two variants for the oxygen chemical schemes. We find that the effective lifetime of H_2O in Titan's atmosphere exceeds 10 yr below 200 km, which is only a factor of six shorter than that of CO_2 when the column densities are averaged. As a consequence, solving the inconsistency between the OH/H_2O fluxes required matching the observed H_2O and CO_2 amounts, which is not straightforward and depends on the magnitude of the flux discrepancy. We find that if the Cottini et al. (2012) measurements are representative of Titan's true H_2O profile, the factor about five in the discrepancy in flux can be solved by invoking a decrease by a factor of ten in the OH/H_2O flux (i.e., of Enceladus' plume activity) over the last ~300 years. While the past activity of Enceladus is unconstrained, the fact that active plumes are currently not emitted along entire tiger stripes fractures and that thermal anomalies are not limited to fractures leaves open the possibility of a more extended and intense activity. If on the other hand, Titan's water is even less abundant by about another factor of four as found by Moreno et al. (2012), we find that the time-dependent flux scenario is not in itself able to solve the problem and that another loss term for H_2O, such as a loss to the haze, has to be invoked.

Acknowledgements. This research has been supported by the Spanish Ministerio de Ciencia e Innovación under contract AyA 2009-08011 and Ministerio de Economía y Competitividad under contract AyA 2012-32237. We thank Ralph D. Lorenz for suggesting the comet impact scenario to us.

References

Adachi, H., Basco, H., & James, D. 1981, Int. J. Chem. Kinet., 13, 1251
Adamson, J., Farhat, S., Morter, C., et al. 1994, J. Phys. Chem., 98, 5665
Ashfold, M., Fullstone, M., Hancock, G., & Ketley, G. 1981, Chem. Phys., 55, 245
Atkinson, R., Baulch, D. L., Cox, R. A., et al. 2004, Atmos. Chem. Phys., 4, 1461
Atkinson, R., Baulch, D. L., Cox, R. A., et al. 2006, Atmos. Chem. Phys., 6, 3625
Balucani, N., Leonori, F., & Casavecchia, P. 2012, Energy, 43, 47
Bartels, M., Edelbüttel-Einhaus, J., & Hoyermann, K. 1991, Symp. Int. Combust. Proc., 23, 131
Baulch, D. L., Cobos, C. J., Cox, R. A., et al. 1992, J. Phys. Chem. Ref. Data, 21, 411

Baulch, D. L., Cobos, C. J., Cox, R. A., et al. 1994, J. Phys. Chem. Ref. Data, 23, 847
Baulch, D., Bowman, C., Cobos, C., et al. 2005, J. Phys. Chem. Ref. Data, 34, 757
Bergeat, A., Moisan, S., Méreau, R., & Loison, J.-C. 2009, Chem. Phys. Lett., 480, 21
Berman, M., Fleming, J., Harvey, A., & Lin, M. 1982, Proc. Combustion Institute, 19, 73
Blitz, M., Pesa, M., Pilling, M., & Seakins, P. 1999, J. Phys. Chem. A, 103, 5699
Böhland, T., Temps, F., & Wagner, H. G. 1984, Z. Electrochem., 88, 1222
Böhland, T., Temps, F., & Wagner, H. G. 1985, Berichte der Bunsengesellschaft für physikalische Chemie, 89, 1013
Böhland, T., Temps, F., & Wagner, H. 1988, Proc. Combustion Institute, 21, 841
Canosa, A., Sims, I. R., Travers, D., Smith, I. W. M., & Rowe, B. R. 1997, A&A, 323, 644
Carl, S. A., Minh Thi Nguyen, H., Elsamra, R. M. I., Tho Nguyen, M., & Peeters, J. 2005, J. Chem. Phys., 122
Cavalié, T., Hartogh, P., Billebaud, F., et al. 2010, A&A, 510, A88
Cavalié, T., Feuchtgruber, H., Lellouch, E., et al. 2013, A&A, 553, A21
Cody, R. J., Romani, P. N., Nesbitt, F. L., et al. 2003, J. Geophys. Res.: Planets, 108, 5
Cottini, V., Nixon, C. A., Jennings, D. E., et al. 2012, Icarus, 220, 855
Coustenis, A., Salama, A., Lellouch, E., et al. 1998, A&A, 336, L85
Cui, J., Yelle, R. V., Vuitton, V., et al. 2009, Icarus, 200, 581
Davidson, J., Schiff, H., Brown, T., & Howard, C. J. 1978, J. Chem. Phys., 69, 1216
Dóbó, S., Bórces, T., & Szilágyi, I. 1991, J. Chem. Soc., Faraday Transactions, 87, 2331
De Avillez Pereira, R., Baulch, D., Pilling, M., Robertson, S., & Zeng, G. 1997, J. Phys. Chem. A, 101, 9681
de Kok, R., Irwin, P. G. J., Teanby, N. A., et al. 2007, Icarus, 186, 354
de La Haye, V., Waite, J. H., Johnson, R. E., et al. 2007, J. Geophys. Res., 112, 7309
Dobrijevic, M., Hébrard, E., Loison, J. C., & Hickson, K. M. 2014, Icarus, 228, 324
Fahr, A., & Laufer, A. 1995, J. Phys. Chem., 99, 262
Fahr, A., Laufer, A., Klein, R., & Braun, W. 1991, J. Phys. Chem., 95, 3218
Feuchtgruber, H., Lellouch, E., de Graauw, T., et al. 1997, Nature, 389, 159
Fu, B., Han, Y.-C., Bowman, J., et al. 2012a, Proc. Nat. Acad. Sci. USA, 109, 9733
Fu, B., Han, Y.-C., Bowman, J., et al. 2012b, J. Chem. Phys., 137, 22A532
Fulchignoni, M., Ferri, F., Angrilli, F., et al. 2005, Nature, 438, 785
Fulle, D., & Hippler, H. 1997, J. Chem. Phys., 106, 8691
Gurwell, M. A. 2004, ApJ, 616, L7
Hack, W., Hold, M., Hoyermann, K., Wehmeyer, J., & Zeuch, T. 2005, Phys. Chem. Chem. Phys, 7, 1977
Hanning-Lee, M. A., & Pilling, M. J. 1992, Int. J. Chem. Kinet., 24, 271
Harding, L., Klippenstein, S., Georgievskii, Y., et al. 2005, Proc. Combustion Institute, 30I, 985
Hassinen, E., Kalliorinne, K., & Koskikallio, J. 1990, Int. J. Chem. Kinetics, 22
Hébrard, E., Dobrijevic, M., Loison, J. C., et al. 2013, A&A, 552, A132
Heinemann, P., Hofmann-Sievert, R., & Hoyermann, K. 1988, Proc. Combustion Institute, 21, 865
Hesman, B. E., Davis, G. R., Matthews, H. E., & Orton, G. S. 2007, Icarus, 186, 342
Hickson, K., Caubet, P., & Loison, J.-C. 2013, J. Phys. Chem. Lett., 4, 2843
Homann, K., & Wellmann, C. 1983, Berichte der Bunsengesellschaft/Physical Chemistry Chemical Physics, 87, 609, 33
Hörst, S. M., Vuitton, V., & Yelle, R. V. 2008, J. Geophys. Res. Planets, 113, 10006
Hoyermann, K., Loftfield, N., Sievert, R., & Wagner, H. 1981, Proc. Combustion Institute, 18, 831
Hoyermann, K., Olzmann, M., Seeba, J., & Viskolcz, B. 1999, J. Phys. Chem. A, 103, 5692
Jasper, A., Klippenstein, S., Harding, L., & Ruscic, B. 2007, J. Phys. Chem. A, 111, 3932
Klemm, R. B. 1979, J. Chem. Phys., 71, 1987
Knyazev, V., & Slagle, I. 2001, J. Phys. Chem. A, 105, 3196
Koyano, I., Wauchop, T. S., & Welge, K. H. 1975, J. Chem. Phys., 63, 110
Krasnoperov, L., Chesnokov, E., Stark, H., et al. 2005, Proc. Combustion Institute, 30 I, 935
Krasnopolsky, V. A. 2009, Icarus, 201, 226
Langford, A. O., Petek, H., & Moore, C. B. 1983, J. Chem. Phys., 78, 6650
Lara, L. M., Lellouch, E., López-Moreno, J. J., & Rodrigo, R. 1996, J. Geophys. Res., 101, 23261
Lara, L.-M., Lellouch, E., & Shematovich, V. 1999, A&A, 341, 312
Laufer, A., & Fahr, A. 2004, Chem. Rev., 104, 2813
Laufer, A., Gardner, E., Kwok, T., & Yung, Y. 1983, Icarus, 56, 560
Lavvas, P. P., Coustenis, A., & Vardavas, I. M. 2008, Planet. Space Sci., 56, 27
Lellouch, E., Bézard, B., Moreno, R., et al. 1997, Planet. Space Sci., 45, 1203
Lellouch, E., Bézard, B., Moses, J. I., et al. 2002, Icarus, 159, 112
Lellouch, E., Moreno, R., & Paubert, G. 2005, A&A, 430, L37
McKay, C. P. 1996, Planet. Space Sci., 44, 741
Monks, P., Nesbitt, F., Payne, W., et al. 1995, J. Phys. Chem., 99, 17151
Moreno, R., Marten, A., Matthews, H. E., & Biraud, Y. 2003, Planet. Space Sci., 51, 591
Moreno, R., Lellouch, E., Lara, L. M., et al. 2012, Icarus, 221, 753
Moses, J., Bézard, B., Lellouch, E., et al. 2000, Icarus, 143, 244
Moses, J. I., Fouchet, T., Bézard, B., et al. 2005, J. Geophys. Res. Planets, 110, 8001
Murhpy, J., Vakhtin, A., & Leone, S. 2003, Icarus, 163, 175
Nava, D. F., Mitchell, M. B., & Stief, L. J. 1986, J. Geophys. Res., 91, 4585
Ohmori, K., Miyoshi, A., Matsui, H., & Washida, N. 1990, J. Phys. Chem., 94, 3253
Okabe, H. 1978, Photochemistry of Small Molecules (New York: Wiley Interscience Publication)
Opansky, B., & Leone, S. 1996a, J. Phys. Chem., 100, 4888
Opansky, B., & Leone, S. 1996b, J. Phys. Chem., 100, 19904
Pereira, R., Baulch, D., Pilling, J., Robertson, S., & Zheng, G. 1997, J. Phys. Chem. A, 101, 9681
Pitts, W. M., Pasternack, L., & McDonald, J. 1982, Chem. Phys., 68, 417
Pratt, G. L., & Wood, S. W. 1984, J. Chem. Soc., Faraday Trans. 1, 80, 3419
Sander, S. P., Friedl, R. R., Ravishankara, A. R., et al. 2006, NASA JPL Publication 06-2
Sander, S. P., Friedl, R. R., Ravishankara, A. R., et al. 2011, NASA JPL Publication 10-6
Sangwan, M., Chesnokov, E., & Krasnoperov, L. 2012, J. Phys. Chem. A, 116, 8661
Schwanebeck, W., & Warnatz, J. 1975, Ber. Bunsenges. Phys. Chem., 79, 530
Shepler, B., Yang, B., Dhilip Kumar, T., et al. 2007, A&A, 475, L15
Tsang, W. 1991, J. Phys. Chem. Ref. Data, 20, 221
Tsang, W., & Hampson, R. 1986, J. Phys. Chem. Ref. Data, 15, 1087
Tully, J. C. 1975, J. Chem. Phys., 62, 1893
Vakhtin, A., Heard, D., Smith, I., & Leone, S. 2001, Chem. Phys. Lett., 348, 21
Vanlook, H., & Peeters, J. 1995, J. Phys. Chem., 99
Vinatier, S., Bézard, B., Fouchet, T., et al. 2007, Icarus, 188, 120
Vinatier, S., Bézard, B., Nixon, C. A., et al. 2010, Icarus, 205, 559
Vinckier, C. 1979, J. Chem. Phys., 83
Wagner, A., & Bowman, J. 1987, J. Phys. Chem., 91, 5314
Wagner, H. G., & Zellner, R. 1972, Ber. Bunsen-Ges. Phys. Chem.
Wang, H., & Frenklach, M. 1997, Combust. Flame, 110, 173
Wang, B., Hou, H., & Gu, Y. 2000, J. Chem. Phys., 112, 8458
Wang, H. Y., Eyre, J. A., & Dorfman, L. M. 1973, J. Chem. Phys., 59
Wilson, E. H., & Atreya, S. K. 2004, J. Geophys. Res. Planets, 109, 6002
Yung, Y. L., Allen, M., & Pinto, J. P. 1984, ApJS, 55, 465
Zabarnick, S., Fleming, J., & Lin, M. 1988, Proc. Combustion Institute, 21, 713
Zahnle, K., Schenk, P., Levison, H., & Dones, L. 2003, Icarus, 163, 263
Zhang, X., Zou, S., Harding, L., & Bowman, J. 2004, J. Phys. Chem. A, 108, 8980
Zhu, R., Xu, Z., & Lin, M. 2004, J. Chem. Phys., 120, 6566
Zwier, T., & Allen, M. 1996, Icarus, 123, 578

Pages 10 to 14 are available in the electronic edition of the journal at http://www.aanda.org

Table 1. Hydrocarbon reactions.

	Reaction	Rate coefficient	Reference
R1a	$^1CH_2 + H_2 \rightarrow CH_3 + H$	9.24×10^{-11}	Langford et al. (1983)
R1b	$^1CH_2 + H_2 \rightarrow ^3 CH_2 + H_2$	1.26×10^{-11}	Langford et al. (1983)
R2	$^1CH_2 + CH_4 \rightarrow CH_3 + CH_3$	6.0×10^{-11}	Böhland et al. (1985)
R3	$CH + CH_4 \rightarrow C_2H_4 + H$	$3.96 \times 10^{-8} T^{-1.04} e^{-36.1/T}$	Canosa et al. (1997)
R4	$CH + H_2 + M \rightarrow CH_3 + M$	$k_0 = 8.75 \times 10^{-31} e^{524/T}$	Moses et al. (2005)
		$k_\infty = 8.3 \times 10^{-11}$	Fulle & Hippler (1997)
R5	$H + CH_3 + M \rightarrow CH_4 + M$	$k_0 = 1.7 \times 10^{-24} T^{-1.8}$	Baulch et al. (1994)
		$k_\infty = 3.5 \times 10^{-10}$	
R6	$CH_3 + CH_3 + M \rightarrow C_2H_6 + M$	$k_0 = 2.822 \times 10^{-3} T^{-8.749} e^{-985.4/T}$	Cody et al. (2003);
		$k_\infty = 9.3132 \times 10^{-11} e^{-1.519 \times 10^{-3} T}$	Lavvas et al. (2008)
R7	$H + H + M \rightarrow H_2 + M$	$k_0 = 1.5 \times 10^{-29} T^{-1.3}$	Tsang & Hampson (1986)
		$k_\infty = 1.0 \times 10^{-11}$	Lavvas et al. (2008)
R8	$H + C_2H_2 + M \rightarrow C_2H_3 + M$	$k_0 = 2.6 \times 10^{-31}$	Baulch et al. (1992)
		$k_\infty = 3.8 \times 10^{-11} e^{-1374/T}$	
R9	$H + C_2H_3 \rightarrow C_2H_2 + H_2$	3.30×10^{-11}	Monks et al. (1995)
R10	$H_2 + C_2H_3 \rightarrow C_2H_4 + H$	$2.6 \times 10^{-13} e^{-2646/T}$	Fahr & Laufer (1995)
R11	$H + C_2H_4 + M \rightarrow C_2H_5 + M$	$k_0 = 2.15 \times 10^{-29} T^{-2} e^{-349/T}$	Baulch et al. (1994)
		$k_\infty = 4.95 \times 10^{-11} e^{-1051/T}$	
R12	$H + C_2H_5 \rightarrow CH_3 + CH_3$	$7.95 \times 10^{-11} e^{-127/T}$	Pratt & Wood (1984)
R13	$^3CH_2 + H + M \rightarrow CH_3 + M$	$k_0 = 3.4 \times 10^{-32} e^{736/T}$	Moses et al. (2000)
		$k_\infty = 7.3 \times 10^{-12}$	
R14	$^3CH_2 + CH_3 \rightarrow C_2H_4 + H$	7.0×10^{-11}	Tsang & Hampson (1986)
R15	$^3CH_2 + C_2H_2 + M \rightarrow CH_3C_2H + M$	$k_0 = 6.0 \times 10^{-29} e^{1680/T}$	Böhland et al. (1988)
		$k_\infty = 2.0 \times 10^{-12} e^{-3330/T}$	
R16	$C_2H + H + M \rightarrow C_2H_2 + M$	$k_0 = 1.26 \times 10^{-18} e^{-721/T}$	Tsang & Hampson (1986)
		$k_\infty = 3.0 \times 10^{-10}$	
R17	$C_2H + H_2 \rightarrow C_2H_2 + H$	$5.58 \times 10^{-11} e^{-1443/T}$	Opansky & Leone (1996b)
R18	$C_2H + CH_4 \rightarrow C_2H_2 + CH_3$	$6.94 \times 10^{-12} e^{-250/T}$	Opansky & Leone (1996a)
R19	$C_2H + C_2H_6 \rightarrow C_2H_2 + C_2H_5$	$5.1 \times 10^{-11} e^{-76/T}$	Murhpy et al. (2003)
R20	$C_2H + C_2H_2 \rightarrow C_4H_2 + H$	1.3×10^{-10}	Vakhtin et al. (2001)
R21	$CH_3C_2H + H \rightarrow CH_3 + C_2H_2$	$9.62 \times 10^{-12} e^{-1560/T}$	Wagner & Zellner (1972)
R22	$CH_3C_2H + H + M \rightarrow_3 H_5 + M$	$k_0 = 8.0 \times 10^{-24} T^{-2} e^{-1225/T}$	Yung et al. (1984)
		$k_\infty = 9.7 \times 10^{-12} e^{-1550/T}$	Wang et al. (2000)
R23	$C_2H_3 + C_2H_3 \rightarrow C_2H_4 + C_2H_2$	3.5×10^{-11}	Laufer & Fahr (2004)
R24	$C_2H_3 + C_2H_3 + M \rightarrow C_4H_6 + M$	$k_0 = 2.822 \times 10^{-3} T^{-8.749} e^{-985.4/T}$	Lavvas et al. (2008)
		$k_\infty = 9.5 \times 10^{-11}$	Laufer & Fahr (2004)
R25	$C_4H + H_2 \rightarrow C_4H_2 + H$	$1.20 \times 10^{-11} e^{-998/T}$	Lavvas et al. (2008)
R26	$C_4H + CH_4 \rightarrow C_4H_2 + CH_3$	$1.2 \times 10^{-11} e^{-491/T}$	Lavvas et al. (2008)
R27	$C_4H + C_2H_6 \rightarrow C_4H_2 + C_2H_5$	$5.1 \times 10^{-11} e^{-76/T}$	Lavvas et al. (2008)
R28	$C_4H + H + M \rightarrow C_4H_2 + M$	$k_0 = 1.26 \times 10^{-18} T^{-3.1} e^{-721/T}$	Moses et al. (2000)
		$k_\infty = 3.0 \times 10^{-10}$	
R29	$CH_4 + C_2H_2 \rightarrow C_6H_2 + H$	1.3×10^{-10}	Lavvas et al. (2008)
R30	$C_4H + C_4H_2 \rightarrow C_8H_2 + H$	$1.1 \times 10^{-10} e^{28/T}$	Moses et al. (2000)
R31	$C_2H + C_4H_2 \rightarrow C_6H_2 + H$	1.3×10^{-10}	Lavvas et al. (2008)
R32	$^*C_4H_2 + C_4H_2 \rightarrow C_8H_2 + H_2$	1.5×10^{-10}	Zwier & Allen (1996)
R33	$C_4H_2 + H \rightarrow C_4H_3$	$1.4 \times 10^{-10} e^{-1184/T}$	Schwanebeck & Warnatz (1975); Nava et al. (1986)
R34a	$C_4H_3 + H \rightarrow C_4H_2 + H_2$	5.0×10^{-12}	Wang & Frenklach (1997)
R34b	$C_4H_3 + H \rightarrow C_2H_2 + C_2H_2$	1.5×10^{-11}	Wang & Frenklach (1997)
R35	$C_2 + H_2 \rightarrow C_2H + H$	$1.77 \times 10^{-10} e^{-1469/T}$	Pitts et al. (1982)
R36	$C_2 + CH_4 \rightarrow C_2H + CH_3$	$5.05 \times 10^{-11} e^{-297/T}$	Pitts et al. (1982)
R37	$C_2H + C_2H_4 \rightarrow C_2H_2 + C_2H_3$	$1.8 \times 10^{-11} e^{-302/T}$	from Lara et al. (1996)
R38	$C_4H + C_2H_4 \rightarrow C_4H_2 + C_2H_3$	1.4×10^{-10}	Vakhtin et al. (2001)
R39	$^1CH_2 + N_2 \rightarrow ^3 CH_2 + N_2$	7.9×10^{-12}	Ashfold et al. (1981)
R40	$^3CH_2 + ^3 CH_2 \rightarrow C_2H_2 + H_2$	3.1×10^{-10}	Baulch et al. (1992)
R41	$C_2H_5 + CH_3 \rightarrow C_2H_4 + CH_4$	$5.04 \times 10^{-14} T^{0.41} e^{429/T}$	Zhu et al. (2004)
R42	$C_2H_5 + CH_3 + M \rightarrow C_3H_8 + M$	$k_0 = 2.822 \times 10^{-3} T^{-8.749} e^{-985.4/T}$	Lavvas et al. (2008)
		$k_\infty = 2.41 \times 10^{-10} T^{-0.34} e^{-259/T}$	Zhu et al. (2004)
R43a	$C_2H_5 + C_2H_3 \rightarrow C_2H_6 + C_2H_2$	2.81×10^{-12}	Tsang & Hampson (1986)
R43b	$C_2H_5 + C_2H_3 \rightarrow C_2H_4 + C_2H_4$	2.81×10^{-12}	Tsang & Hampson (1986)
R44	$C_2H_5 + C_2H_5 \rightarrow C_2H_6 + C_2H_4$	2.3×10^{-12}	Baulch et al. (1992)
R45	$C_2H_5 + C_2H_5 + M \rightarrow C_4H_{10} + M$	$k_0 = 6.723 \times 10^{-11} T^{-4.534}$	Laufer et al. (1983); Baulch et al. (1992)
		$k_\infty = 1.8 \times 10^{-11}$	
R46	$C_3H_3 + H + M \rightarrow CH_3C_2H + M$	$k_0 = 5.5 \times 10^{-27}$	Moses et al. (2000)
		$k_\infty = 2.5 \times 10^{-10}$	Homann & Wellmann (1983)

Table 1. continued.

	Reaction	Rate coefficient	Reference
R47a	$C_3H_5 + H \rightarrow CH_3C_2H + H_2$	1.5×10^{-11}	Hanning-Lee & Pilling (1992)
R47b	$C_3H_5 + H \rightarrow CH_2CCH_2 + H_2$	1.5×10^{-11}	Hanning-Lee & Pilling (1992)
R48a	$C_3H_5 + CH_3 \rightarrow CH_3C_2H + CH_4$	4.5×10^{-12}	Tsang (1991)
R48b	$C_3H_5 + CH_3 \rightarrow CH_2CCH_2 + CH_4$	4.5×10^{-12}	Tsang (1991)
R49	$C_3H_2 + H + M \rightarrow C_3H_3 + M$	$k_0 = 2.52 \times 10^{-28}$ $k_\infty = 5.0 \times 10^{-11}$	Moses et al. (2000)
R50	$^3CH_2 + C_2H_2 \rightarrow C_3H_3 + H$	$2.00 \times 10^{-11} e^{-3332/T}$	Tsang & Hampson (1986)
R51	$C_3H_8 + C_2H \rightarrow C_2H_2 + C_3H_7$	$9.8 \times 10^{-11} e^{-71/T}$	Murhpy et al. (2003)
R52	$C_2H_3 + CH_3 + M \rightarrow C_3H_6 + M$	$k_0 = 6.0 \times 10^{-28} e^{1680/T}$ $k_\infty = 1.2 \times 10^{-10}$	Fahr et al. (1991)
R53	$C_3H_5 + H + M \rightarrow C_3H_6 + M$	$k_0 = 2.0 \times 10^{-28}$ $k_\infty = 1.0 \times 10^{-11}$	Moses et al. (2000) Hanning-Lee & Pilling (1992)
R54	$C_2H_3 + CH_3 \rightarrow C_2H_2 + CH_4$	3.4×10^{-11}	Fahr et al. (1991)
R55	$C_2H_3 + C_2H_5 + M \rightarrow C_4H_8 + M$	$k_0 = 2.822 \times 10^{-3} T^{-8.749} e^{-985.4/T}$ $k_\infty = 6.5 \times 10^{-11}$	Lavvas et al. (2008) Laufer & Fahr (2004)
R56	$C_3H_5 + CH_3 + M \rightarrow C_4H_8 + M$	$k_0 = 2.822 \times 10^{-3} T^{-8.749} e^{-985.4/T}$ $k_\infty = 1.55 \times 10^{-9} T^{-0.54} e^{117/T}$	Lavvas et al. (2008) Knyazev & Slagle (2001)
R57	$C_4H_2 + H + M \rightarrow C_4H_3 + M$	$k_0 = 1.0 \times 10^{-28}$ $k_\infty = 1.39 \times 10^{-10} e^{-1184/T}$	Schwanebeck & Warnatz (1975) Nava et al. (1986)
R58	$^*C_4H_2 \rightarrow C_4H_2 + h\nu$	1.0×10^3	Zwier & Allen (1996)
R59	$CH + C_2H_4 \rightarrow CH_3C_2H + H$	$3.87 \times 10^{-9} T^{-0.55} e^{-29.6/T}$	Canosa et al. (1997)

Table 2. Hörst et al. (2008) C-H-O reactions.

	Reaction	Rate coefficient	Reference
R60	$O(^1S) \rightarrow O(^3D)$	1.3×10^{0}	Koyano et al. (1975)
R61	$O(^1D) \rightarrow O(^3P)$	6.7×10^{-3}	Okabe (1978)
R62	$O(^1D) + N_2 \rightarrow O(^3P) + N_2$	$2.2 \times 10^{-11} e^{110/T}$	Sander et al. (2006)
R63	$O(^1D) + H_2 \rightarrow OH + H$	1.1×10^{-10}	Sander et al. (2006)
R64a	$O(^1D) + CH_4 \rightarrow OH + CH_3$	1.1×10^{-10}	Sander et al. (2006)
R64b	$O(^1D) + CH_4 \rightarrow CH_3O + H$	3.0×10^{-11}	Sander et al. (2006)
R64c	$O(^1D) + CH_4 \rightarrow H_2CO + H_2$	7.5×10^{-12}	Sander et al. (2006)
R65a	$O(^1D) + CO \rightarrow O(^3P) + CO$	$4.7 \times 10^{-11} e^{63/T}$	Davidson et al. (1978)
R65b	$O(^1D) + CO \rightarrow CO_2$	8.0×10^{-11}	Tully (1975)
		1.0×10^{-30}	Hörst et al. (2008)
R66a	$O(^3P) + CH_3 \rightarrow HCHO + H$	6.9×10^{-11}	Hack et al. (2005)
R66b	$O(^3P) + CH_3 \rightarrow CO + H_2 + H$	5.7×10^{-11}	Hack et al. (2005)
R67a	$O(^3P) + HCO \rightarrow CO_2 + H$	5.0×10^{-11}	Baulch et al. (1992)
R67b	$O(^3P) + HCO \rightarrow CO + OH$	5.0×10^{-11}	Baulch et al. (1992)
R68a	$O(^3P) + CH_3CO \rightarrow CO_2 + CH_3$	2.6×10^{-10}	Baulch et al. (1992)
R68b	$O(^3P) + {}^1CH_2 \rightarrow CH_2CO + OH$	6.4×10^{-11}	Baulch et al. (1992)
R69	$OH + H_2 \rightarrow H_2O + H$	$7.7 \times 10^{-12} e^{-2100/T}$	Atkinson et al. (2004)
R70	$OH + {}^3CH_2 \rightarrow HCHO + H$	3.0×10^{-11}	Tsang & Hampson (1986)
R71a	$OH + CH_3 \rightarrow H_2O + {}^1CH_2$	$6.4 \times 10^{-8} T^{5.8} e^{485/T}$	Pereira et al. (1997)
		$1.8 \times 10^{-8} T^{-0.91} e^{-275/T}$	Pereira et al. (1997)
R71b	$OH + CH_3 \rightarrow HCHO + H_2$	$1.1 \times 10^{-17} T^{8.0} e^{1240/T}$	Pereira et al. (1997)
		$3.8 \times 10^{-14} T^{-0.12} e^{209/T}$	Pereira et al. (1997)
R71c	$OH + CH_3 \rightarrow CH_3OH$	$7.2 \times 10^{-9} T^{-0.79}$	Pereira et al. (1997)
		$1.1 \times 10^{-10} T^{-6.21} e^{-671/T}$	Pereira et al. (1997)
R72	$OH + CH_4 \rightarrow H_2O + CH_3$	$1.9 \times 10^{-12} e^{-1690/T}$	Atkinson et al. (2006)
R73	$OH + C_2H_2 \rightarrow CH_3CO$	$9.2 \times 10^{-18} T^{2}$	Sander et al. (2006)
		5.5×10^{-30}	Sander et al. (2006)
R74	$OH + C_2H_4 \rightarrow HOCH_2CH_2$	$1.1 \times 10^{-9} T^{-0.85}$	Sander et al. (2006)
		$1.4 \times 10^{-17} T^{-4.5}$	Sander et al. (2006)
R75a	$OH + CO \rightarrow CO_2 + H$	$1.4 \times 10^{-13} (1 + [N_2]/4.2 \times 10^{19})$	Atkinson et al. (2006)
R75b	$OH + CO \rightarrow HOCO$	$1.8 \times 10^{-9} T^{-1.3}$	Sander et al. (2006)
		$2.0 \times 10^{-36} T^{1.4}$	Sander et al. (2006)
R76	$HCO + H \rightarrow CO + H_2$	1.5×10^{-10}	Baulch et al. (1992)
R77	$HCO + CH_3 \rightarrow CO + CH_4$	2.0×10^{-10}	Tsang & Hampson (1986)
R78	$CH_3O + H \rightarrow HCHO + H_2$	3.0×10^{-11}	Baulch et al. (1992)
R79	$CH_3O + CH_3 \rightarrow HCHO + CH_4$	4.0×10^{-11}	Tsang & Hampson (1986)
R80a	$CH_3CO + CH_3 \rightarrow CO + C_6H_6$	5.4×10^{-11}	Adachi et al. (1981)
R80b	$CH_3CO + CH_3 \rightarrow CH_2CO + CH_4$	1.0×10^{-11}	Hassinen et al. (1990)
R80c	$CH_3CO + CH_3 \rightarrow CH_3COCH_3$	7.0×10^{-11}	Hassinen et al. (1990)
		1.0×10^{-30}	Hörst et al. (2008)
R81	$C_2H + H_2O \rightarrow OH + C_2H_2$	$2.1 \times 10^{-12} e^{-200/T}$	Vanlook & Peeters (1995)

Table 3. Simplified set of C-H-O reactions derived from Dobrijevic et al. (2014, see text).

	Reaction	Rate coefficient	Reference
R60	$O(^1D) + N_2 \rightarrow O(^3P) + N_2$	$2.15 \times 10^{-11} e^{110/T}$	Sander et al. (2011)
R61	$O(^1D) + H_2 \rightarrow OH + H$	1.1×10^{-10}	Sander et al. (2011)
R62a	$O(^1D) + CH_4 \rightarrow OH + CH_3$	1.05×10^{-10}	Atkinson et al. (2006)
R62b	$O(^1D) + CH_4 \rightarrow CH_3O + H$	3.5×10^{-11}	Atkinson et al. (2006)
R62c	$O(^1D) + CH_4 \rightarrow H_2CO + H_2$	7.5×10^{-12}	Atkinson et al. (2006)
R63a	$O(^3P) + CH_3 \rightarrow H_2CO + H$	1.1×10^{-10}	Baulch et al. (2005); Dobrijevic et al. (2014)
R63b	$O(^3P) + CH_3 \rightarrow CO + H + H_2$	2.9×10^{-11}	Baulch et al. (2005); Dobrijevic et al. (2014)
R64a	$O(^3P) + {}^1CH_2 \rightarrow HCO + H$	1.0×10^{-11}	Böhland et al. (1984); Vinckier (1979);
R64b	$O(^3P) + {}^1CH_2 \rightarrow CO + H + H$	5.0×10^{-11}	Shepler et al. (2007); Wang et al. (1973);
R64c	$O(^3P) + {}^1CH_2 \rightarrow CO + H_2$	6.0×10^{-11}	Baulch et al. (2005); Zhang et al. (2004)
R65a	$O(^3P) + {}^3CH_2 \rightarrow HCO + H$	1.0×10^{-11}	Böhland et al. (1984); Vinckier (1979);
R65b	$O(^3P) + {}^3CH_2 \rightarrow CO + H + H$	5.0×10^{-11}	Shepler et al. (2007); Wang et al. (1973);
R65c	$O(^3P) + {}^3CH_2 \rightarrow CO + H_2$	6.0×10^{-11}	Baulch et al. (2005); Zhang et al. (2004)
R66a	$O(^3P) + C_2H_2 \rightarrow {}^3CH_2 + CO$	$6.6 \times 10^{-12} e^{-1600/T}$	Baulch et al. (2005); Sander et al. (2011)
R66b	$O(^3P) + C_2H_2 \rightarrow HC_2O + H$	$2.6 \times 10^{-11} e^{-1600/T}$	Baulch et al. (2005); Sander et al. (2011)
R67a	$O(^3P) + C_2H_4 \rightarrow CH_3CO + H$	$4.8 \times 10^{-13} (T/300)^{1.88} e^{-92/T}$	Baulch et al. (2005); Fu et al. (2012a,b); Balucani et al. (2012)
R67b	$O(^3P) + C_2H_4 \rightarrow CH_3 + HCO$	$5.0 \times 10^{-13} (T/300)^{1.88} e^{-92/T}$	Baulch et al. (2005); Fu et al. (2012a,b); Balucani et al. (2012)
R67c	$O(^3P) + C_2H_4 \rightarrow {}^3CH_2 + H_2CO$	$1.0 \times 10^{-13} (T/300)^{1.88} e^{-92/T}$	Baulch et al. (2005); Fu et al. (2012a,b); Balucani et al. (2012)
R67d	$O(^3P) + C_2H_4 \rightarrow CH_2CO + H_2$	$3.0 \times 10^{-14} (T/300)^{1.88} e^{-92/T}$	Baulch et al. (2005); Fu et al. (2012a,b); Balucani et al. (2012)
R68a	$O(^3P) + C_2H_3 \rightarrow CH_3 + CO$	6.0×10^{-11}	Heinemann et al. (1988); Harding et al. (2005); Dobrijevic et al. (2014)
R68b	$O(^3P) + C_2H_3 \rightarrow OH + C_2H_2$	1.0×10^{-11}	Heinemann et al. (1988); Harding et al. (2005); Dobrijevic et al. (2014)
R69a	$O(^3P) + C_2H_5 \rightarrow H_2CO + CH_3$	5.0×10^{-11}	Harding et al. (2005); Hoyermann et al. (1999)
R69b	$O(^3P) + C_2H_5 \rightarrow CH_3CHO + H$	6.0×10^{-11}	Harding et al. (2005); Hoyermann et al. (1999)
R69c	$O(^3P) + C_2H_5 \rightarrow OH + C_2H_4$	3.0×10^{-11}	Harding et al. (2005); Hoyermann et al. (1999)
R70	$O(^3P) + C_4H_2 \rightarrow CO + C_3H_2$	$1.31 \times 10^{-11} e^{-678/T}$	Adamson et al. (1994)
R71	$OH + H_2 \rightarrow H_2O + H$	$2.8 \times 10^{-12} e^{-1800/T}$	Sander et al. (2011)
R72a	$OH + CH_3 \rightarrow H_2O + {}^1CH_2$	3.2×10^{-11}	De Avillez Pereira et al. (1997); Jasper et al. (2007); Sangwan et al. (2012)
R72b	$OH + CH_3 \rightarrow H_2CO + H_2$	8.0×10^{-12}	De Avillez Pereira et al. (1997); Jasper et al. (2007); Sangwan et al. (2012)
R72c	$OH + CH_3 \rightarrow CH_3OH$	$k_0 = 2.0 \times 10^{-26} (T/300)^{-6} e^{-1000/T}$	
		$k_\infty = 1.2 \times 10^{-10} (T/300)^{-0.49}$	De Avillez Pereira et al. (1997); Jasper et al. (2007); Sangwan et al. (2012)
R73	$OH + CH_4 \rightarrow H_2O + CH_3$	$1.9 \times 10^{-12} e^{-1690/T}$	Atkinson et al. (2006)
R74	$OH + C_2H_2 \rightarrow CH_3CO$	$k_0 = 5.5 \times 10^{-30}$	Sander et al. (2011)
		$k_\infty = 8.3 \times 10^{-13} (T/300)^2$	Sander et al. (2011)
R75	$OH + C_2H_4 \rightarrow HOCH_2CH_2$	$k_0 = 1.0 \times 10^{-28} (T/300)^{-4.5}$	Sander et al. (2011)
		$k_\infty = 7.5 \times 10^{-12} (T/300)^{-0.85}$	Sander et al. (2011)
R76	$OH + CO \rightarrow CO_2 + H$	$1.68 \times 10^{-13} e^{-30/T} [1 + e^{-T/161} \frac{N_2}{7.8 \times 10^{18} T}]$	Atkinson et al. (2006)
R77	$HCO + H \rightarrow CO + H_2$	1.5×10^{-10}	Baulch et al. (2005)
R78	$HCO + CH_3 \rightarrow CO + CH_4$	9.3×10^{-11}	Krasnoperov et al. (2005); Hébrard et al. (2013)
R79a	$H + CH_3O \rightarrow CH_3 + OH$	3.0×10^{-12}	Hoyermann et al. (1981); Dóbó et al. (1991)
R79b	$H + CH_3O \rightarrow H_2CO + H_2$	3.0×10^{-11}	Hoyermann et al. (1981); Dóbó et al. (1991)

Table 3. continued.

	Reaction	Rate coefficient	Reference
R80	$CH_3O + CH_3 \rightarrow H_2CO + CH_4$	4.0×10^{-11}	Tsang & Hampson (1986)
R81	$C_2H + H_2O \rightarrow OH + C_2H_2$	$7.9 \times 10^{-24}(T/300)^{3.05}e^{-376/T}$	Carl et al. (2005)
R82	$H + CO \rightarrow HCO$	$k_0 = 7.5 \times 10^{-35}(T/300)^{0.2}$	Baulch et al. (2005)
		$k_\infty = 1.2 \times 10^{-10}e^{-1000/T}$	Wagner & Bowman (1987); Wang et al. (1973)
R83	$H + H_2CO \rightarrow H_2 + HCO$	$3.3 \times 10^{-11}e^{-1850/T}$	Klemm (1979)
R84a	$H + CH_3CO \rightarrow CH_3 + HCO$	4.0×10^{-11}	Bartels et al. (1991); Ohmori et al. (1990)
R84b	$H + CH_3CO \rightarrow H_2C_2O + H_2$	2.0×10^{-11}	Bartels et al. (1991); Ohmori et al. (1990)
R85	$CH + H_2O \rightarrow H_2CO + H$	$2.8 \times 10^{-11}(T/300)^{-1.22}e^{-12/T}$	Blitz et al. (1999); Bergeat et al. (2009); Hickson et al. (2013); Zabarnick et al. (1988)
R86	$CH + H_2CO \rightarrow H_2C_2O + H$	$1.0 \times 10^{-10}e^{-260/T}$	Zabarnick et al. (1988)
R87	$CH + CO_2 \rightarrow H + CO + CO$	$5.71 \times 10^{-12}e^{-345/T}$	Berman et al. (1982)
R88	$CH_3 + CH_3O \rightarrow CH_4 + H_2CO$	4.0×10^{-11}	Tsang & Hampson (1986)